



Electrostatically mediated selectivity of Pd nanocatalyst via rectifying contact with semiconductor: Replace ligands with light

Tian-Jian Zhao, Wei-Jie Feng, Jun-Jun Zhang, Bing Zhang, Yong-Xing Liu, Yun-Xiao Lin, Hong-Hui Wang, Hui Su, Xin-Hao Li*, Jie-Sheng Chen*

School of Chemistry and Chemical Engineering, Shanghai Jiao Tong University, Shanghai 200240, People's Republic of China

ARTICLE INFO

Keywords:

Rectifying contact
Photogenerated electric field
Hydrogenation
Furfural

ABSTRACT

Noble metal-based heterogeneous catalysts usually suffered from limited strategies for modifying their selectivity as compared with the homogeneous counterparts. Herein, we reported the electrostatically mediated selectivity of Pd nanocatalyst of usual supported Pd nanoparticles for total hydrogenation of furfural by enhancing the interfacial electric field using visible light and a rectifying contact with semiconductive supports to promote preferred adsorption of C=O groups of furfural to the Pd side. This concept-new approach showed the potential to replace traditional organic ligands with light. The Pd nanoparticles deposited on a semiconductor support, optimized to be g-C₃N₄ (Pd/CN) in this work, exhibits outstanding selectivity ($\geq 97\%$) to tetrahydrofurfuryl alcohol, far surpassing the selectivity of reported single-phase Pd nanocatalysts.

1. Introduction

Noble metal-based catalysts show high catalytic activity in many reactions with widely applications in the fine chemistry [1–8]. The rational design of myriad amounts of organic ligands to modify the activity and selectivity of metal centers has been well demonstrated in the homogeneous catalytic system, however difficult separation and reusability would result in serious environmental issues [9–12]. Within the regards to real applications in industry and fine chemistry, heterogeneous catalysts are preferred due to their good to excellent reusability and thus relatively lost cost for large-scale uses [13]. Effective strategies for modifying the activity and/or selectivity of heterogeneous Pd nanocatalysts are however still rather limited at the moment. Moreover, the rational control in the selectivity of nanocatalysts for multi-step reactions [14,15], taking the hydrogenation of furfural as a model reaction in this work, has been considered as the key approach to significant depressing the cost of separation or purification for mass production of the target products, but has been less touched till now.

Surface modification strategies have been utilized to tailor the selectivity of noble metal nanoparticles (e.g. Pd nanoparticles) by introducing shape-selective zeolite coatings, specific acid-base nanocomposites of metal oxides or active organic addlayers [16–22]. Precisely control in the crystalline facet and interface of bimetallic structure could also result in unexpected high selectivity of the Pd-based nanocatalysts, even though the complex synthetic methods are

not suitable for mass production of these catalysts [23]. Recently, external electric field has been recently applied to trigger the Diels–Alder reaction of conjugated diene and dienophile at the single-molecule level over an Au tip of scanning tunneling microscopy, promising a huge room to further widen the scope of electrostatic-mediated strategy for modifying the activity of metal centers [24]. Herein, we described a photogenerated electric field-mediated approach to tailoring the selectivity of supported Pd nanoparticles with an optimized semiconductive catalyst support for highly efficient hydrogenation of furfural to tetrahydrofurfuryl alcohol in water. This environmentally friendly approach showed the potential to replace traditional organic ligands with light. The rectifying contact between Pd metal and the semiconductor (exemplified with g-C₃N₄ here) could spontaneously initiate the electron redistribution at their interface, which can be further enhanced by the visible light irradiation due to the interfacial Schottky barrier. The enhanced electric field at the Pd-support interface could facilitate the selective adsorption of C=O of furfural on its surface, ensuring the final selectivity to the target product tetrahydrofurfuryl alcohol. Moreover, the ease of mass production, low cost and high chemical stability of g-C₃N₄ benefit the applications of the Pd/g-C₃N₄ nanocomposites as real catalysts for artificial synthesis and even hydrogen production [25–34].

Considering the practical applications of potential heterogeneous nanocatalysts for mass production, a sustainable hydrogenation path of furfural required less energy consumption, zero emission and green

* Corresponding authors.

E-mail addresses: xinhaoli@sjtu.edu.cn (X.-H. Li), chemcj@sjtu.edu.cn (J.-S. Chen).

<https://doi.org/10.1016/j.apcatb.2018.07.048>

Received 17 April 2018; Received in revised form 30 June 2018; Accepted 15 July 2018

Available online 17 July 2018

0926-3373/© 2018 Elsevier B.V. All rights reserved.

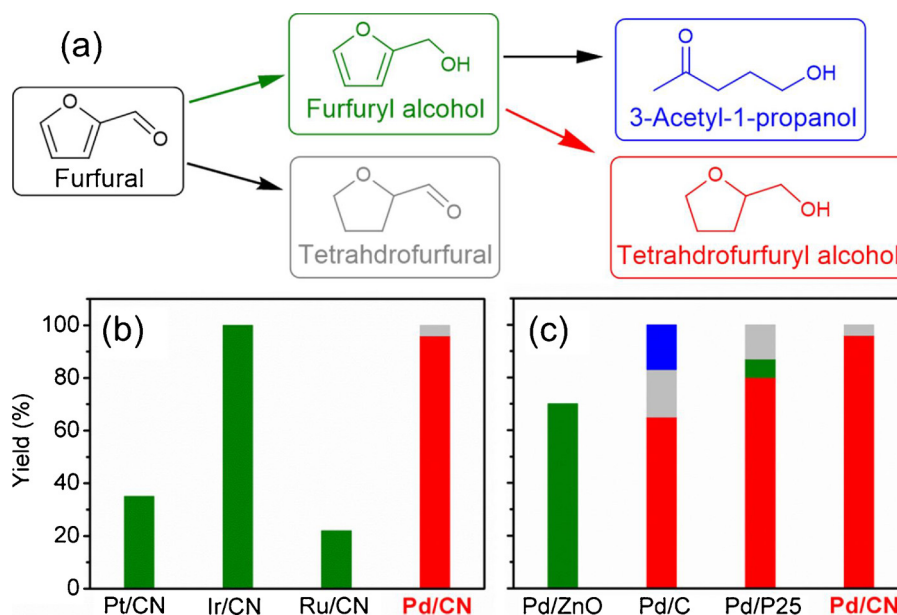


Fig. 1. Screening catalysts for hydrogenation of furfural. (a) Illustration of reaction routes for the hydrogenation of furfural; (b) Screening catalysts with varied metal components (b) and supports (c). Reaction conditions: furfural (0.25 mmol), 8 wt% catalyst (20 mg), H₂O (5 mL), H₂ (1 bar), 8 h, room temperature.

solvents and reactants [35–37]. To this end, we evaluated the catalytic performance of all catalysts for room-temperature and additive-free reactions using water as the solvent and hydrogen gas as the hydrogen source. As presented in Fig. 1a, the hydrogenation of furfural under mild conditions gave at least four products [38–40] among which the furfuryl alcohol was the only product commercial available [29]. As a product of total hydrogenation of furfural, the tetrahydrofurfuryl alcohol was preferred as an organic solvent with less toxic and higher stability or a more processable precursor for the production of bio-fuel [41]. Unfortunately, the selectivity to tetrahydrofurfuryl alcohol over various single-phase noble metal nanocatalysts was still not satisfied at the moment.

2. Experimental section

2.1. Synthesis of mesoporous CN [42–44]

Firstly, 5 g of cyanamide was dissolved in 15 g of Ludox HS40 solution (dispersion of 14 nm SiO₂ particles with 40 wt% in water). The as-formed solution was fast added with ethanol to form white gel. Then the white colloid was placed into crucible and heated at a temperature of 550 °C for 4 h (ramp: 2.3 °C/min) under the protection of N₂ atmosphere. The yellow powders were etched with HF acid (final concentration: 4 M) for one day to remove the silica template. Then the powders were centrifuged, washed three times with distilled water and once with ethanol and finally dried at 60 °C overnight.

2.2. Synthesis of 8 wt% Pd/CN

The as-prepared mesoporous g-C₃N₄ (CN, 100 mg) was dispersed into 40 mL of distilled water with 15 mg of PdCl₂ under stir for 12 h. 4 M NaOH solution was added to adjust the pH of the solution to 13. Then, 60 mg NaBH₄ was dissolved in 10 mL water and dropped into the as-preparation solution quickly. The solution was stirred for 6 h. Finally, the catalyst was separated by centrifugation and washed with water and ethanol in sequence, and then dried at 60 °C overnight.

2.3. Synthesis of 8 wt% Pt/CN, 8 wt% Ru/CN and 8 wt% Ir/CN

The as-prepared mesoporous g-C₃N₄ (CN, 100 mg) was dispersed

into 40 mL of distilled water with 23.94 mg of H₂PtCl₆·6H₂O, 18.44 mg of RuCl₃ or 13.98 mg of IrCl₃ under stir for 12 h. 4 M NaOH solution was added to adjust the pH of the solution to 13. Then, 60 mg NaBH₄ was dissolved in 10 mL water and dropped into the as-preparation solution quickly. The solution was stirred for 6 h. Finally, the catalyst was separated by centrifugation and washed with water and ethanol in sequence, and then dried at 60 °C overnight.

2.4. Synthesis of 8 wt% Pd/C, 8 wt% Pd/P25 and 8 wt% Pd/ZnO

The catalyst support (100 mg), including carbon (Vulcan XC 72, Cabot), P25 and ZnO, was separately dispersed into 40 mL of distilled water with 15 mg of PdCl₂ under stir for 12 h. 4 M NaOH solution was added to adjust the pH of the solution to 13. Then, 60 mg NaBH₄ was dissolved in 10 mL water and dropped into the as-preparation solution quickly. The solution was stirred for 6 h. Finally, the catalyst was separated by centrifugation and washed with water and ethanol in sequence, and then dried at 60 °C overnight.

2.5. Preparation of CN and Pd/CN electrode and test

To prepare electrodes, 1.5 mg catalyst and 80 μL of 5 wt% Nafion solutions were dispersed in 1.5 mL of ethanol. The as-prepared mixture was sonicated for 2 h to form a homogeneous ink. Then, 50 μL of catalyst ink was dropped on FTO glasses (1*2 cm²) for twice. After dried up, the FTO glasses were placed in an oven at 120 °C for 1 h. Nafion was not added for the test of Mott-Schottky curves.

2.6. Preparation of CN and Pd/CN electrode and test

The tests of photocurrent responses and Mott-Schottky curves were performed on electrochemistry workstation (CHI660E, China) using a three-electrode electrochemical quartz cell in a 0.5 M Na₂SO₄ solution under simulated sunlight illumination (Perfectlight Tech. Co., Ltd., PLS-SXE300C, 300 W Xe lamp) using long-pass cutoff filters to control the wavelength. The three-electrode electrochemical cell was consisted of Pd/CN or CN, Pt coil and a saturated calomel electrode (SCE), served as working electrode, counter electrode, and reference electrode, respectively. Electrolyte was saturated with N₂ gas before the measurements. And the measured potentials versus SCE were all converted to the

reversible hydrogen electrode scale according to the Nernst equation. The photocurrent responses of Pd/CN as various wavelengths on and off were measured at 1 V and Mott–Schottky Plots was performed from -1.35 V to -1.1 V.

3. Density functional theory (DFT) calculations

All theoretical calculations were performed using density functional theory (DFT), as implemented in the DMol3 program. The electronic exchange-correlation energy was described by the generalized gradient approximation (GGA) method with spin polarized Perdew–Burke–Ernzerhof (PBE) functional with TS dispersion correction. Valence orbitals were described with the double numerical plus polarization (DNP) basis. The orbital cutoff is 4.5 \AA . Density functional semicore pseudopotentials (DSPPs) was used for metals. In adsorption calculations, the k-space integration was sampled using a $3 \times 3 \times 1$ Monkhorst-Pack grid. In the adsorption models, a large box ($14.21 \times 14.21 \times 27.14 \text{ \AA}^3$), is used to calculate the adsorption of furfural at the interface of the Pd/CN and Pd/C. One layer of carbon nitride (graphene) is placed at the bottom of the box. A Pd_8 cluster is placed about 2 \AA right above the support plane. The vacuum layer thickness is set to be 19.2 \AA . Atoms in carbon nitride and palladium are relaxed in the calculation. Structural optimization were obtained on the basis of convergence criterion that SCF tolerance was 10^{-5} Ha, and convergence tolerances of energy, maximum force, and maximum displacement applied during geometry optimization were 2×10^{-5} Ha, 0.004 Ha/\AA , and 0.005 \AA , respectively. Smearing was used to accelerate convergence with the value of 0.002 . The adsorption energy of the substrate molecule is calculated using equation S1:

$$E_{\text{ads}} = E_{\text{Pd}} + E_{\text{sub}} - E_{\text{tot}} \quad (1)$$

where E_{ads} , E_{Pd} , E_{sub} , E_{tot} represents the adsorption energy, energies of palladium-carbon nitride complex, furfural and palladium-carbon nitride complex adsorbed furfural respectively.

4. Results and discussion

Both the noble metals and the catalysts supports were initially optimized for the hydrogenation of furfural to tetrahydrofurfuryl alcohol in this work (Fig. 1a–c and Table S1–3). All supported noble metal nanocatalysts with varied semiconductive catalyst supports were prepared by conventional wet impregnation method. Transmission electron microscopy (TEM) observation (Figure S2) directly indicates the success in depositing Pd nanoparticles on the surface of CN support without the formation of free-standing Pd nanoparticles. Further High-resolution transmission electron microscopy (HRTEM) image of the Pd nanoparticles supported on CN with good crystallinity and an ultra-small size between $3\text{--}5 \text{ nm}$ further demonstrates the key role of the strong coupling effect of CN support with Pd species in stabilizing the as-formed Pd nanoparticles. With the same catalyst support, fixed metal loadings (8 wt\%) and similar particle size (Figure S2–3), Pd/CN exhibited the highest yield of the tetrahydrofurfuryl alcohol among the Pd, Pt, Ru and Ir-based nanocatalysts (Fig. 1b). Further optimization on the catalyst support suggested the graphitic carbon nitride ($\text{g-C}_3\text{N}_4$ or CN) as the best semiconductive catalyst support to significantly promote the selectivity to tetrahydrofurfuryl alcohol over the Pd nanocatalysts without the formation of obvious over-reduced byproducts as detected in the products over Pd/C (Fig. 1c and Figure S4). Other inorganic semiconductors also showed more or less improvement in the final selectivity to tetrahydrofurfuryl alcohol, rather suggesting the key role of the semiconductive catalyst supports in modifying the Pd nanoparticles into more selective and milder nanocatalysts here. Since Pd/CN was the best catalyst for the total hydrogenation of furfural, it was used in subsequent characterizations and experiments.

Further calculation on the adsorption structure (Fig. 2a and Fig. S6), strongly related to the hydrogenation selectivity/activity, was carried

out to demonstrate the real role of the electric field at the boundary of Pd/CN in promoting the selectivity to tetrahydrofurfuryl alcohol. Generally speaking, the pre-adsorption of the furfural molecules on the surface metal nanoparticles was mainly via the C=O site and/or furan ring, where the catalyst support was usually considered as a mechanical support, for example, in the system of Pd/C (Fig. 2a).

However, the as-formed electric field induced by the charge redistribution at the boundary of Pd/CN via a rectifying contact [25–29] obviously decrease the adsorption energies (Fig. 2a) of furfural and thus facilitate the reactivity of adsorbed furfural for further hydrogenation. Most importantly, the dyadic boundary of the electron-rich (light red in Fig. 2a) Pd and electron-deficient (light green in Fig. 2a) $\text{g-C}_3\text{N}_4$ enhanced the adsorption of furan ring by attract its electrons to the surface of $\text{g-C}_3\text{N}_4$ support, resulted in coupled complexes as marked by a red ring in corresponding charge density difference (CDD) stereograms (Fig. 2a insets) [45].

Simultaneously, a preferred adsorption of the C=O site to the Pd side of the Pd/CN model could be expected for further hydrogenation via furfuryl alcohol to tetrahydrofurfuryl alcohol. This theoretical simulation result well explained the highly depressed conversion of furfural to tetrahydrofurfuryl alcohol under mild conditions applied and remained as a byproduct in this work (Fig. 1a) [38]. The preferred adsorption of the C=O site to Pd nanoparticles in the Pd/CN was also confirmed by the even enlarged difference (13.8 kcal/mol) between the two adsorption structures over the Pd/CN as compared with that (5.7 kcal/mol) over Pd/C.

Further temperature programmed desorption (TPD) analysis results (Fig. 2b) of furfural also suggested a relatively lower desorption temperature and thus a lower adsorption energy over the Pd/CN as compared to Pd/C, matching well with the trend revealed by the theoretical calculation results (Fig. 2a). Meanwhile, the TPD results of furfuryl alcohol (Fig. S7) and tetrahydrofurfuryl alcohol (Fig. 2c) indicated that tetrahydrofurfuryl alcohol could detach easily from the surface of Pd/CN, depressing the possibility of further conversion of tetrahydrofurfuryl alcohol into unwanted byproducts. A linear relationship between the adsorption capacity of furfural molecules (Fig. 2d and Table S4) and Pd contents of the Pd/CN catalysts from 3% to 8% with well dispersed Pd nanoparticles (Fig. S8) was observed. The selective adsorption of furfural molecules to the surface of Pd in Pd/CN catalysts was further confirmed via Diffuse reflectance FT-IR spectroscopy (DRIFT) analysis (Figure S9) with typical signal of C=O detected only for 8% Pd/CN sample [46]. Most importantly, the elevated desorption temperature but lowered adsorption capacity of furfural over the Pd/CN- 10% sample with highly aggregated Pd nanoparticles (Fig. S8) exhibited the worst selectivity among all Pd/CN catalysts and only comparable to that over the Pd/C catalyst (Fig. 2e). All these results experimentally demonstrated the key role of the boundaries of Pd/CN heterojunction in modifying the preferred adsorption of the substrate and thus facilitating the selective transformation.

One typical way to further enhance the electron-hole separation at the rectifying interface of $\text{g-C}_3\text{N}_4$ and Pd for better activity and/or selectivity (Fig. 3a–b) was to generate additional charge carriers using light irradiation and thus a build-in electric field at the interface due to the presence of Schottky barrier (Fig. 3c) [21–25]. Surprisingly, the reaction time for the total hydrogenation of furfural to tetrahydrofurfuryl alcohol was shortened from 8 to 2 h simply by applying a visible light irradiation (Fig. 3a and S10) even though the hydrogenation of furfural didn't consume photo-generated electrons at all. The similar trends of wavelength-dependent yields (Fig. 3b) of the tetrahydrofurfuryl alcohol and photocurrent intensities (Fig. 3d) by Pd/CN catalyst directly demonstrated the connection between the improved selectivity of the Pd/CN dyad and the photo-generated interfacial electric field.

The photo-induced strengthen in the interfacial electric further confirmed by the gradual enhanced band bending of the CN

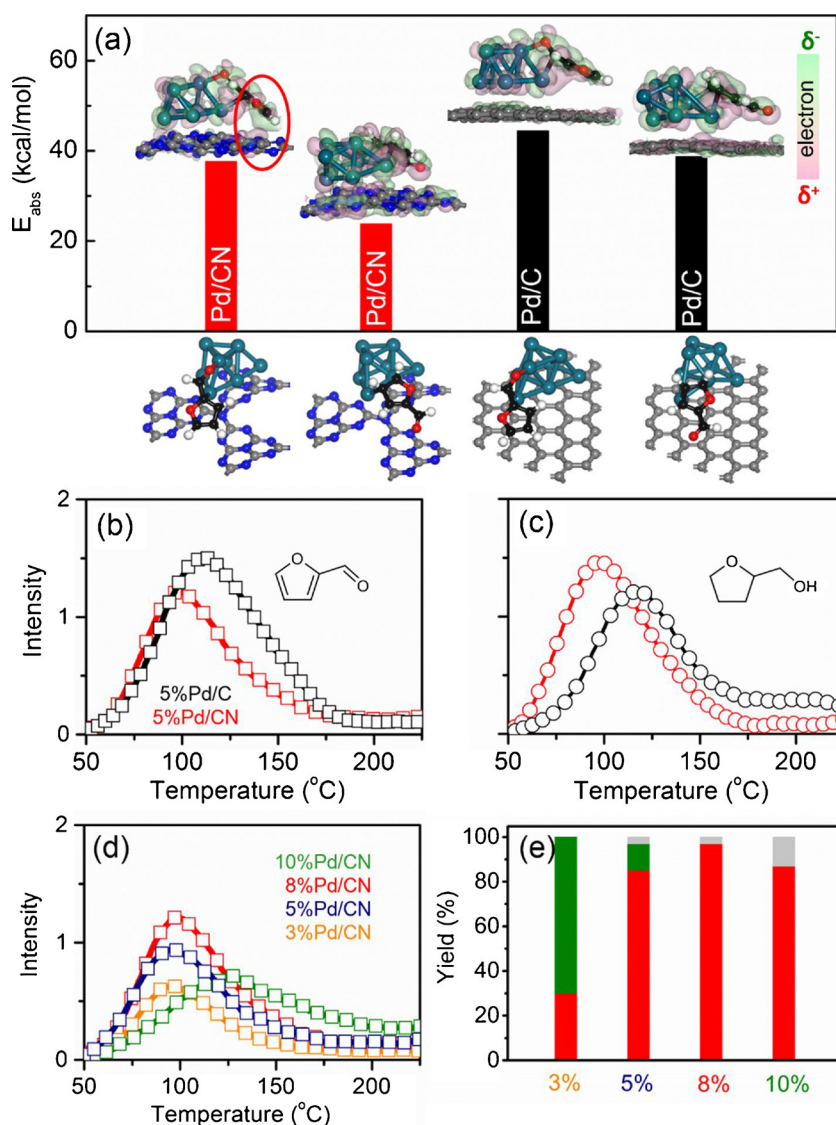


Fig. 2. Effect of rectifying contact on enhanced selectivity. (a) Calculated structures (bottom) and adsorption energies (bars) of furfural with C=O (left) and furan ring (right) adsorbed on Pd clusters supported on g-C₃N₄ (red bars) or carbon (black bars). Insets: CDD stereograms after the adsorption of a furfural molecule onto the model. TPD profiles of furfural (b) and tetrahydrofurfuryl alcohol (c) over the Pd/CN (red lines) and Pd/C (black lines) catalysts (Pd content: ~ 8%). TPD profiles (d) of furfural over Pd/CN catalysts with varied Pd contents and corresponding yields (e) of tetrahydrofurfuryl alcohol (red bars), furfuryl alcohol (olive bars) and tetrahydrofurfural (grey bars).

components in Pd/CN, estimated from corresponding Mott-Schottky curves (Fig. 3e) under the irradiation of light rays with even shorter wavelength, as compared to the band position of pristine CN (Fig. 3f). It should be noted that long-pass cutoff filters were used in this work to control the wavelength of the light. As a result, the total intensity of the illumination and thus possible numbers of electron-hole pairs decrease with the wavelength of filters used. If more electrons are initiated and donated from the semiconductor (CN) to the metal side due to Schottky barrier at the metal-semiconductor interface, the band bending will be further enlarged, resulting in even lower valence and conduction band position. In combination with the DFT calculation and TPD analysis results (Fig. 2), all these results well explained the decreased yields of tetrahydrofurfural in the final products from 4% to less than 2% (Fig. 3b) under light irradiation via a more preferred adsorption of C=O of furfural on Pd surface as the proposed reaction mechanism (Fig. 4) in this work. Pd/CN exhibited a much higher selectivity to tetrahydrofurfuryl alcohol (97%) under milder conditions than those of all reported noble metal-based heterogeneous catalysts in the literature (Table S6).

The photo-induced interfacial electric field between Pd and g-C₃N₄ could also be generally applied for selective hydrogenation of furfural and substituted furfurals (Table S7), including 5-methylfurfural, 5-chloro-2-furaldehyde, 2,5-diformylfuran and 5-hydroxymethylfurfural, with excellent tolerance of functional groups. Moreover, the

recyclability of the Pd/CN catalyst was demonstrated by the stable activity (Figure S13) and structure (Figure S14) of the reused catalyst for three cycles. We also monitored the Pd content in the mother solution of the catalytic reaction by Inductively Coupled Plasma Optical (ICP) analysis. The fact that the possible amount of Pd leached to the solution is even lower than the detection limit of the ICP facilitate (data not shown), again indicates the high stability of the Pd/CN catalyst during the reaction.

5. Conclusions

In summary, we described an alternative approach to controlling the selectivity of usual supported Pd nanoparticles for selective hydrogenation of furfural to tetrahydrofurfuryl alcohol by constructing a rectifying contact between Pd metal and g-C₃N₄ which showed the potential to replace traditional organic ligands with light. Such a rectifying contact between Pd metal and the semiconductor could initiate the formation of a static electric field via electron redistribution at their interface (which can be further enhanced by visible light irradiation) and facilitate the selective adsorption of C=O of furfural to the Pd cluster, ensuring the high selectivity to total hydrogenation product tetrahydrofurfuryl alcohol. This work demonstrated a new strategy to control the final selectivity of semiconductor-embedded metal-based nanocatalysts using only solar ray, promising sustainable methods for

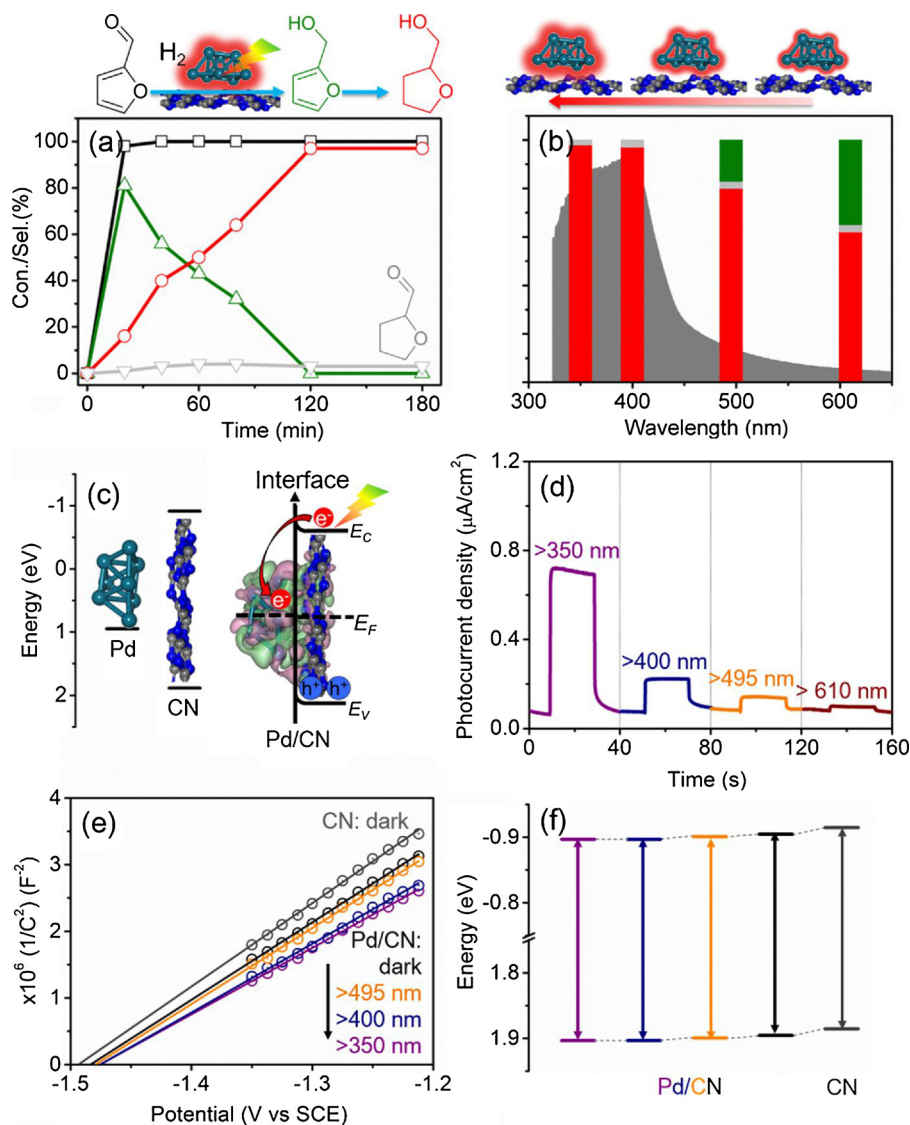


Fig. 3. Light mediated selectivity. (a) Typical time course of furfural hydrogenation over Pd/CN and corresponding selectivity to various products under visible light ($\lambda > 400$ nm). (b) Wavelength-dependent selectivity (bars) for furfural hydrogenation by Pd/CN, matching well with trend of the light absorption of the CN support (dark grey area). The yield of tetrahydrofurfural (grey bar) was depressed to less than 3% in the products. (c) Schematic model of the Mott-Schottky-type rectifying contact in Pd/CN. (d) Photocurrent responses of Pd/CN electrodes initiated by light with different wavelength. Mott-schottky curves (e) and estimated energy band structure of bare CN and Pd/CN in dark and under light irradiation.

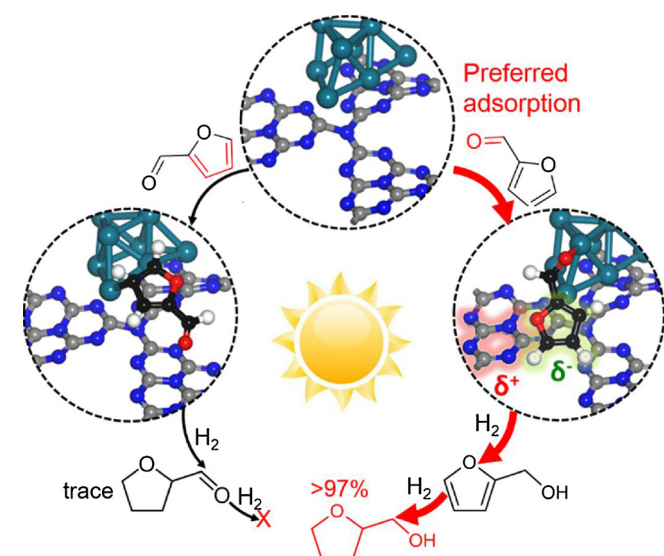


Fig. 4. Proposed reaction pathway for the high selectivity to tetrahydrofurfuryl alcohol over Pd/CN catalyst under light irradiation.

organic synthesis and bio-fuel production in water.

Conflict of interest

The authors declare no competing financial interest.

Acknowledgments

This work was supported by National Nature Science Foundation of China (21720102002, 21722103 and 21673140), Shanghai Basic Research Program (16JC1401600), SJTU-MPI partner group, Shanghai Eastern Scholar Program and Shanghai Rising-Star Program (16QA1402100).

Appendix A. Supplementary data

Supplementary material related to this article can be found, in the online version, at doi:<https://doi.org/10.1016/j.apcatb.2018.07.048>.

References

- [1] E.A.B. Kantchev, C.J. O'Brien, M.G. Organ, *Angew. Chem. Int. Ed.* 46 (2007) 2768.
- [2] D.I. Enache, J.K. Edwards, P. Landon, B. Solsona-Espriu, A.F. Carley, A.A. Herzing, M. Watanabe, C.J. Kiely, D.W. Knight, G.J. Hutchings, *Science* 311 (2006) 362.
- [3] J. Xu, J.K. Shang, Y. Chen, Y. Wang, Y.X. Li, *Appl. Catal. A: Gen.* 542 (2017) 380.

- [4] Z.Z. Zhang, M.K. Xu, W.K. Ho, X.W. Zhang, Z.Y. Yang, X.X. Wang, *Appl. Catal. B: Environ.* 184 (2015) 174.
- [5] S.S. Stahl, *Angew. Chem. Int. Ed.* 43 (2004) 3400.
- [6] J.W. Sun, Y.S. Fu, G.Y. He, X.Q. Sun, X. Wang, *Appl. Catal. B: Environ.* 165 (2015) 661.
- [7] A. Kolmakov, D.O. Klenov, Y. Lilach, S. Stemmer, M. Moskovits, *Nano Lett.* 5 (2005) 667.
- [8] R.A. Rather, S. Singh, B. Pal, *Appl. Catal. B: Environ.* 213 (2017) 9.
- [9] J.E. Bercaw, N. Hazari, J.A. Labinger, P.F. Oblad, *Angew Chem Int. Ed.* 47 (2008) 9941.
- [10] S. Fantasia, J.D. Egbert, V. Jurčík, C.S.J. Cazin, H. Jacobsen, L. Cavallo, M. Heinekey, S.P. Nolan, *Angew Chem Int. Ed.* 48 (2009) 5182.
- [11] R.E. Rodríguez-Lugo, M. Trincado, M. Vogt, F. Tewes, G. Santiso-Quinones, H. Grützmacher, *Nat. Chem.* 5 (2013) 342.
- [12] M. Costa, P. Pelagatti, C. Pelizzi, D. Rogolino, *J. Mol. Catal. A: Chem.* 178 (2002) 21.
- [13] D. Astruc, F. Lu, J.R. Aranzas, *Angew. Chem. Int. Ed.* 44 (2005) 7852.
- [14] S.M. Rogers, C.R.A. Catlow, C.E. Chan-Thaw, A. Chutia, N. Jian, R.E. Palmer, M. Perdjon, A. Thetford, N. Dimitratos, A. Villa, P.P. Wells, *ACS Catal.* 7 (2017) 2266.
- [15] M.J. Taylor, L.J. Durndell, M.A. Isaacs, C.M.A. Parlett, K. Wilson, A.F. Lee, G. Kyriakou, *Appl. Catal. B: Environ.* 180 (2016) 580.
- [16] T.L. Cui, W.Y. Ke, W.B. Zhang, H.H. Wang, X.H. Li, J.S. Chen, *Angew. Chem. Int. Ed.* 55 (2016) 9178.
- [17] J. Zhang, L. Wang, Y. Shao, Y. Wang, B.C. Gates, F.S. Xiao, *Angew. Chem. Int. Ed.* 56 (2017) 1.
- [18] L. Zhuang, H.X. Li, W.L. Dai, M.H. Qiao, *Chem. Lett.* 32 (2003) 1072.
- [19] M.H. Ab Rahim, M.M. Forde, R.L. Jenkins, C. Hammond, Q. He, N. Dimitratos, J.A. Lopez-Sanchez, A.F. Carley, S.H. Taylor, D.J. Willock, D.M. Murphy, C.J. Kiely, G.J. Hutchings, *Angew. Chem. Int. Ed.* 52 (2013) 1280.
- [20] C. Rameshan, W. Stadlmayr, C. Weilach, S. Penner, H. Lorenz, M. Hävecker, R. Blume, T. Rocha, D. Teschner, A. Knop-Gericke, R. Schlögl, N. Memmel, D. Zemlyanov, G. Rupprechter, B. Klötzer, *Angew. Chem. Int. Ed.* 49 (2010) 3224.
- [21] H.B. Zhang, X.K. Gu, C. Canlas, A.J.K. Payoli Aich, J.P. Greeley, J.F. Elam, R.J. Meyers, J.A. Dumesic, P.C. Stair, C.L. Marshall, *Angew. Chem. Int. Ed.* 53 (2014) 12132.
- [22] T. Mitsudome, Y. Takahashi, S. Ichikawa, T. Mizugaki, K. Jitsukawa, K. Kaneda, *Angew. Chem. Int. Ed.* 52 (2013) 1481.
- [23] H. Lee, *RSC Adv.* 4 (2014) 41017.
- [24] A.C. Aragonès, N.L. Haworth, N. Darwish, S. Ciampi, N.J. Bloomfield, G.G. Wallace, I. Diez-Perez, M.L. Coote, *Nature* 531 (2016) 88.
- [25] Y.Y. Cai, X.H. Li, Y.N. Zhang, X. Wei, K.X. Wang, J.S. Chen, *Angew Chem. Int. Ed.* 52 (2013) 11822.
- [26] X.H. Li, Y.Y. Cai, L.H. Gong, W. Fu, K.X. Wang, H.L. Bao, X. Wei, J.S. Chen, *Chem.-Eur. J.* 20 (2014) 16732.
- [27] H. Su, K.X. Zhang, B. Zhang, H.H. Wang, Q.Y. Yu, X.H. Li, M. Antonietti, J.S. Chen, *J. Am. Chem. Soc.* 139 (2017) 811.
- [28] X.H. Li, M. Antonietti, *Chem. Soc. Rev.* 42 (2013) 6593.
- [29] J.D. Xiao, L. Han, J. Luo, S.H. Yu, H.L. Jiang, *Angew. Chem. Int. Ed.* 57 (2018) 1103.
- [30] Y. Zheng, L. Liu, X. Ye, F.S. Guo, X.C. Wang, *Angew. Chem. Int. Ed.* 53 (2014) 11926.
- [31] R. Kuriki, H. Matsunaga, T. Nakashima, K. Wada, A. Yamakata, O. Ishitani, K. Maeoda, *J. Am. Chem. Soc.* 138 (2016) 5159.
- [32] Z.Z. Lin, X.C. Wang, *Angew. Chem. Int. Ed.* 52 (2013) 1735.
- [33] Y.Y. Wang, W.J. Yang, X.J. Chen, J. Wang, Y.F. Zhu, *Appl. Catal. B: Environ.* 220 (2018) 337.
- [34] S.B. Wang, J.L. Lin, X.C. Wang, *Phys. Chem. Chem. Phys.* 16 (2014) 14656.
- [35] Q.L. Wei, F.Y. Xiong, S.S. Tan, L. Huang, E.H. Lan, B. Dunn, L.Q. Mai, *Adv. Mater.* 29 (2017) 1602300.
- [36] L. Zhou, Z.C. Zhuang, H.H. Zhao, M.T. Lin, D.Y. Zhao, L.Q. Mai, *Adv. Mater.* 29 (2017) 3696.
- [37] C.D. Liang, Z.J. Li, S. Dai, *Angew. Chem. Int. Ed.* 47 (2008) 3696.
- [38] Y. Nakagawa, K. Takada, M. Tamura, K. Tomishige, *ACS Catal.* 4 (2014) 2718.
- [39] L. Bui, H. Luo, W.R. Gunther, Y. Román-Leshkov, *Angew. Chem. Int. Ed.* 52 (2013) 8022.
- [40] R.F. Ma, X.P. Wu, T. Tong, Z.J. Shao, Y.Q. Wang, X.H. Liu, Q. Xia, X.Q. Gong, *ACS Catal.* 7 (2017) 333.
- [41] K. Yan, G. Wu, T. Lafleur, C. Jarvis, *Renew. Sust. Energy Rev.* 38 (2014) 663.
- [42] X.C. Wang, K. Maeda, X.F. Chen, K. Takanabe, K. Domen, Y.D. Hou, X.Z. Fu, M. Antonietti, *J. Am. Chem. Soc.* 131 (2009) 1680.
- [43] F. Goettmann, A. Thomas, M. Antonietti, *Angew. Chem. Int. Ed.* 46 (2007) 2717.
- [44] F. Goettmann, A. Fischer, A. Thomas, M. Antonietti, *Angew. Chem. Int. Ed.* 45 (2006) 4467.
- [45] T.M. Su, Z.Z. Qin, G. Huang, H.B. Ji, Y.X. Jiang, J.H. Chen, *Appl. Surf. Sci.* 378 (2016) 270.
- [46] M. Rogojerova, G. Kereszturyb, B. Jordanov, *Spectrochimica. Acta Part A* 61 (2005) 1661.